Applied Catalysis B: Environmental 134–135 (2013) 333–343

Contents lists available at SciVerse ScienceDirect

Applied Catalysis B: Environmental

journal homepage: www.elsevier.com/locate/apcatb

Photocatalytic oxidation of propene in gas phase at low concentration by optimized TiO_2 nanoparticles

M. Ouzzine, M.A. Lillo-Ródenas*, A. Linares-Solano

Grupo de Materiales Carbonosos y Medio Ambiente, Dpto. Química Inorgánica, Facultad de Ciencias, Universidad de Alicante, Ap. 99, E-03080 Alicante, Spain

ARTICLE INFO

Article history:
Received 2 October 2012
Received in revised form 10 January 2013
Accepted 21 January 2013
Available online 28 January 2013

Keywords:
Titanium dioxide
Sol–gel method
Photocatalyst
Propene

ABSTRACT

In the present study, nanocrystalline titanium dioxide (TiO_2) was prepared by sol–gel method at low temperature from titanium tetraisopropoxide (TTIP) and characterized by different techniques (gas adsorption, XRD, TEM and FTIR). Variables of the synthesis, such as the hydrolyzing agent (acetic acid or isopropanol) and calcination temperatures (300–800 °C), were analyzed to get uniform size TiO_2 nanoparticles. The effect that these two variables have on the structure of the resultant TiO_2 nanoparticles and on their photocatalytic activity is investigated. The photocatalytic activities of TiO_2 nanoparticles were evaluated for propene oxidation at low concentration (100 ppmv) under two different kinds of UV light (UV-A ~ 365 nm and UV-C ~ 257.7 nm) and compared with Degussa TiO_2 P-25, used as reference sample. The results show that both hydrolyzing agents allow to prepare TiO_2 nanoparticles and that the hydrolyzing agent influences the crystalline structure and its change with the thermal treatments. Interestingly, the prepared TiO_2 nanoparticles possess anatase phase with small crystalline size, high surface area and higher photocatalytic activity for propene oxidation than commercial TiO_2 (Degussa P-25) under UV-light. Curiously, these prepared TiO_2 nanoparticles are more active with the 365 nm source than with the 257.7 nm UV-light, which is a remarkable advantage from an application point of view. Additionally, the obtained results are particularly good when acetic acid is the hydrolyzing agent at both wavelengths used, possibly due to the high crystallinity, low anatase phase size and high surface oxygen groups' content in the nanoparticles prepared with it, in comparison to those prepared using isopropanol.

1. Introduction

In order to obey the different regulations that governments of many countries have issued to protect our atmosphere, a large number of effluent gas cleaning processes have been developed. Most of them make use of classical catalyst materials, like metals or metal oxides, which become catalytically active only at high temperatures. From an economical point of view, the use of this type of catalysts is less profitable in situations where the concentration of the hazardous components in the gas stream is only of some hundreds of ppm and the temperature of the gas is near room temperature. Since under these conditions autothermic operation is not possible, an external heat source is needed to heat the effluent gas stream to reaction temperature [1]. One way to avoid this disadvantage is the use of heterogeneous photocatalytic oxidation (PCO) in presence of UV or near-UV illumination. In this way, PCO is considered to be a promising technology to decompose at ambient temperature some organic compounds, rendering non-toxic products (e.g. H_2O and CO_2) and, in some cases, simple mineral acids [2,3].

Thus, a wide variety of volatile organic compounds (VOCs) such as alkanes [4–6], alkenes [6,7], aromatics [8,9], oxygenates [9] and trichloroethylene [10] have been successfully oxidized at ambient conditions over TiO_2 under UV or near-UV radiation using air or oxygen as oxidants. Among the different VOCs, propene is considered a highly polluting molecule because of its high POCP (photochemical ozone creativity potential) [11,12]. Moreover, propene is one of the major sources of indoor air pollution due to it is one of the principal components of tobacco smoke, together with other alkenes [13]. Surprisingly, few results have been reported about the photocatalytic oxidation of propene over TiO_2 catalysts [14], reason why our research has been dealing with it for some time [15–19].

Among various oxide semiconductor photocatalysts, titania (TiO_2) has proved to be the most suitable one for several reasons: biological and chemical inertness, strong oxidizing power, low cost, and long-term stability against photocorrosion and chemical corrosion [20,21].

Most studies have shown that photocatalytic activity of titanium dioxide is strongly dependent on several parameters such as the UV-source and TiO_2 phase structure (anatase, rutile and brookite, a

* Corresponding author. Tel.: +34 965909350; fax: +34 965903454.
E-mail address: mlillo@ua.es (M.A. Lillo-Ródenas).

0926-3373/$ – see front matter © 2013 Elsevier B.V. All rights reserved.
http://dx.doi.org/10.1016/j.apcatb.2013.01.035

minoritary product of most synthesis [22]). However, controversial results have been reported in the literature regarding their influence.

In relation to the importance of the UV-light, it should be recalled that PCO with TiO_2 requires the use of ultraviolet light to initiate the catalytic reactions; this energy input creates an electronic destabilization of the catalyst which, for example, is in the order of 3.2 eV for the anatase phase [23,24]. Thus, UV-light can be classified according to the wavelength of its main emission band in three groups; UV-light A (365 nm), B (312 nm) and C (250 nm) [25]. A nice example showing the importance of the type of UV-light used when studying the degradation of a dye in presence of TiO_2 under the three types of UV-lights can be found in the literature [26].

In relation to the dependence of the photocatalyst performance of TiO_2 with its crystal composition there are also controversial results [27,28]. Most authors state that anatase works better than rutile [29–31], others found better photocatalytic activity for rutile [32,33] and some detected synergistic effects in the photocatalytic activity for anatase–rutile mixed phases [34,35]. Additionally, other TiO_2 features influence its photocatalytic activity, such as crystal size [36,37] and surface structure [38,39] (like surface hydroxyl groups, oxygen vacancies, etc.).

In relation to all these results, it is desirable to prepare TiO_2 materials with good crystallinity, small grain size and high specific surface area to improve photocatalytic activity. For this purpose, many processes are available, such as ultrasonic irradiation [40], hydrothermal synthesis [41], solvothermal method [42], precipitation method [43] or thermal decomposition of alkoxides [44]. Among the preparation methods, sol–gel has been the most widely employed to prepare TiO_2 nanoparticles because of its simplicity and low equipment requirement [45,46]. However, such method renders amorphous TiO_2 with low photocatalytic activity [45]. Hence, generally it needs to be calcined to form a crystalline material (containing anatase and/or rutile) [47]. The high temperatures required for calcination seriously affect the particle size and surface structure and can result in collapse of the mesoporous structure and low photocatalytic activity [48].

The present work deals with the preparation, by sol–gel method at low temperature (100 °C), of nanocrystalline TiO_2 with anatase phase and high surface area using titanium tetraisopropoxide as the titanium precursor. The influence that the hydrolyzing agent and the thermal treatment have on the physico-chemical properties of TiO_2 nanoparticles and their photocatalytic activity has been studied. Gas phase oxidation of propene at room temperature and at low concentration (100 ppmv) under two UV-light sources has been selected to analyze the effect of this parameter on the photocatalytic activities.

2. Experimental

2.1. Materials

Titanium(IV) isopropoxide (TTIP, 97%), glacial acetic acid (AA, 99%) and isopropanol (IP, 99.5%) were purchased from Sigma–Aldrich and used as such without further purification. Distilled water was used throughout the experimental.

2.2. Preparation of titanium dioxide powders

Nanosized TiO_2 particles were prepared using sol–gel method. A typical synthesis procedure is as follows: titanium(IV) isopropoxide, glacial acetic acid or isopropanol and distilled water were maintained in a molar ratio 1:10:350. Titanium(IV) isopropoxide was hydrolyzed using glacial acetic acid or isopropanol at 0 °C. Distilled water was added drop wise to the solution under vigorous stirring for 1 h. Subsequently, the solution was ultrasonicated for 30 min and continued the stirring for further 5 h until a clear solution of TiO_2 nanocrystals was formed. After this period, the solution was placed in an oven at a temperature of 70 °C, maintained for a period of 12 h for aging process. The gel was then dried at 100 °C and, subsequently, the catalyst was crushed into fine powder [49]. Some of these samples, referred to as "without thermal treatment samples", have been calcined in a muffle furnace at different temperatures, from 300 to 800 °C, at heating rate of 10 °C/min, maintaining this temperature for 5 h to examine the effect of thermal treatment temperature.

The following nomenclature has been used for the samples prepared with acetic acid (TiO_2-AA) or isopropanol (TiO_2-IP). After this, the nomenclature includes the temperatures for thermal treatment, where WT means without treatment, or there is a number that indicates the calcination temperature in °C (i.e. TiO_2-AA-300 has been prepared by acetic acid using 300 °C as thermal treatment temperature).

2.3. Characterization of TiO_2

The crystal phase composition and crystallinity of the obtained TiO_2 nanoparticles was determined by X-ray diffraction (XRD) analysis using a SEIFERT 2002 equipment. Cu Kα (1.54 Å) radiation was used. The scanning velocity was 2°/min, and diffraction patterns were recorded in the angular 2θ range of 6–80°. The crystalline size was estimated by applying the Scherrer's equation [50] using the full width at half-maximum (FWHM) data of the major diffraction peak and a K factor of 0.93:

$$B = \frac{K\lambda}{\beta \cos\theta} \quad (1)$$

where B is the crystalline size (nm); K is the constant whose value is 0.93; λ is the wavelength for the radiation source used, which is 1.54056 Å for Cu Kα; β is the full width at half maximum intensity (FWHM) (radians) and θ is the Bragg angle at the position of the peak maximum.

The content of anatase was also calculated applying Spurr–Myers equation, as shown in Eq. (2) [51]:

$$W_A = \frac{1}{1 + 1.26 I_R/I_A} \quad (2)$$

$$W_R(\%) + W_A(\%) = 100 \quad (3)$$

where W_A is the weight fraction of anatase in the mixture; W_R is the weight fraction of rutile in the mixture; I_R is the intensity of the diffraction peak of rutile and I_A is the intensity of the diffraction peak of anatase.

The specific BET surface area (S_{BET}) and total micropore volume (V_{N_2}) were determined by applying the Brunauer–Emmett–Teller (BET) equation, and the Dubinin–Raduskevich equation to the N_2 adsorption data at −196 °C, respectively, using an Autosorb-6B apparatus from Quantachrome [52]. The volume of narrow micropores (V_{CO_2}) was determined by application of the Dubinin-Radushkevich equation to the CO_2 adsorption data at 0 °C [53], measured using an Autosorb-6B apparatus from Quantachrome. All the samples were degassed at 250 °C for 4 h prior to adsorption experiments. Pore volume and average pore size were determined by nitrogen adsorption volume at a relative pressure of 0.99.

Pore size distributions for all the samples were obtained applying the Barrett–Joynet–Halenda (BJH) formula to the N_2 desorption branch data from the adsorption isotherms at −196 °C, using the software provided by Quantachrome.

Table 1
Textural properties of TiO_2-AA nanoparticles prepared by sol–gel method after different thermal treatment temperatures.

Sample	S_{BET} (m^2/g)	V_{N_2} (cm^3/g)	V_{CO_2} (cm^3/g)	Total pore volume (cm^3/g)	Mean pore size (nm)
TiO_2-AA-WT	271	0.10	0.06	0.30	4.44
TiO_2-AA-300	154	0.06	0.04	0.28	6.90
TiO_2-AA-400	95	0.04	0.03	0.17	7.12
TiO_2-AA-500	24	0.01	0.005	0.06	10.69
TiO_2-AA-600	2	0.001	–	0.01	39.32
TiO_2-AA-700	3	0.001	–	0.01	20.23
TiO_2-AA-800	2	0.001	–	0.01	25.66
TiO_2-P25	55	0.02	0.01	0.18	7.57

The morphology of TiO_2 nanoparticles was observed by transmission electron microscopy (TEM) using INCA Energy TEM100 equipment from Oxford Instruments.

Fourier transform infrared (FTIR) spectra of TiO_2-nanoparticles were recorded in the wavenumber range from 400 to 4000 cm^{-1} using ATI Mattson Infinity Spectrometer. All the FTIR spectra of TiO_2 nanoparticles were collected in transmission mode.

3. Photocatalytic activities

The photocatalytic performance of the different materials was studied using an experimental system designed in our laboratory. The system consists of a vertical quartz reactor where the photocatalyst bed is placed on quartz wool. The reactor is 50 mm height, its diameter is 20 mm and the quartz wool support height is around 10 mm. A UV lamp is placed parallel to the quartz reactor, at a distance around 1 cm. The UV lamp radiation peak appears at 257.7 nm (UV-C) and 365 nm (UV-A), respectively. The commercial references of these lamps are TUV 8W FAM and TL 8W/05 FAM, both from Philips. Their emission powers are 2.1 and 1 W, respectively, as indicated by the manufacturer. Finally, the couple quartz reactor-lamp is surrounded by a cylinder covered by tinfoil. A scheme of this system is detailed elsewhere [15].

The weight of photocatalyst used in these experiments was 0.11 g for all the samples. The photocatalysts were used for the oxidation of propene at 100 ppmv in air at room temperature, 25 °C. The calibrated gas cylinder was supplied by Carburos Metálicos, S.A. Different flow rates of the VOC stream, 30 and 60 ml/min (STP), were tested. These flow rates were controlled by mass flow controllers.

The VOC stream passed through the photocatalyst bed and, afterwards, to a mass spectrometer (Balzers, Thermostar GSD 301 01). After suitable calibrations, the mass spectrometer permits to follow the evolution of the concentration of propene in the outlet gas with time. VOC conversion was calculated using the flowing expression:

$$\text{Propene converesion}\ (\%) = \frac{C_{\text{initial C3H6}} - C_{\text{stationary C3H6}}}{C_{\text{initial C3H6}}} \times 100 \quad (4)$$

where $C_{\text{initial C3H6}}$ is the initial propene concentration, 100 ppmv and $C_{\text{stationary C3H6}}$ is the stationary propene concentration in the photocatalyst bed outlet gas when the UV light is switched-on.

The amount of CO_2 after the oxidation was quantified by mass spectrometry, using a calibrated CO_2-cylinder with a concentration of 300 ppmv.

Additionally, photolysis tests were performed in the same experimental conditions as the catalytic tests but in absence of the TiO_2 photocatalysts, and no photolysis was detected.

4. Results and discussion

In the following section, the characterization of the TiO_2 nanoparticles and their photocatalytic activity for propene oxidation at low concentration is discussed.

4.1. Porosity characterization

The TiO_2 nanoparticles prepared in this work were characterized in terms of porosity. Tables 1 and 2 summarize the textural characteristics of the TiO_2 nanoparticles prepared using acetic acid (TiO_2-AA) or isopropanol (TiO_2-IP), respectively. From them, the effect of calcination temperature on the physical properties of the samples can be analyzed. Increasing the calcination temperature, the specific surface area and the micropore volume drastically and steadily decrease for the two series. Thus, samples TiO_2-AA and TiO_2-IP, that have only been submitted to a drying process at 100 °C, show very large S_{BET} values (271 and 256 m^2/g, respectively), whereas the 800 °C heat treatment reduces their surface area to only 2 m^2/g. Contrarily, with the heat treatment temperature the low mean pore sizes of the untreated samples (4.44 nm and 5.08 nm for TiO_2-AA-WT and TiO_2-IP-WT, respectively) considerably increase (to 25.66 nm and 22.62 nm for TiO_2-AA-800 and TiO_2-IP-800, respectively) due to the growing of the particle sizes.

4.2. XRD analysis

The XRD has been used to investigate the changes of phase structures in the TiO_2 samples. Calcination is a common treatment that can be used to improve the crystallinity of TiO_2 powders. When the powders are calcined at high temperatures, the transformations such as amorphous to anatase and anatase to rutile occur. The amorphous–anatase transformation is complete in the temperature range from 300 to 400 °C [54], whereas the anatase–rutile transformation has been reported to occur in different temperature

Table 2
Textural properties of TiO_2-IP nanoparticles prepared by sol–gel method after different thermal treatment temperatures.

Sample	S_{BET} (m^2/g)	V_{N_2} (cm^3/g)	V_{CO_2} (cm^3/g)	Total pore volume (cm^3/g)	Mean pore size (nm)
TiO_2-IP-WT	256	0.1	0.05	0.32	5.08
TiO_2-IP-300	147	0.06	0.03	0.29	7.93
TiO_2-IP-400	90	0.03	0.02	0.22	9.62
TiO_2-IP-500	28	0.01	0.006	0.12	15.16
TiO_2-IP-600	2	0.001	–	0.01	24.87
TiO_2-IP-700	–	–	–	0.01	19.35
TiO_2-IP-800	–	–	–	0.01	22.62

Table 3
Crystalline size and phase composition of TiO_2-AA samples.

Sample	Phase composition	Anatase by XRD (%)	Rutile by XRD (%)	Crystalline size of anatase (nm)[a]	Crystalline size of rutile (nm)[a]
TiO_2-AA-WT	A	100	–	7	–
TiO_2-AA-300	A	100	–	10	–
TiO_2-AA-400	A	100	–	12	–
TiO_2-AA-500	A	100	–	21	–
TiO_2-AA-600	A-R	75	25	32	35
TiO_2-AA-700	A-R	8	92	44	42
TiO_2-AA-800	R	–	100	–	43
TiO_2-P25	A-R	70	30	20	31

[a] Estimated from XRD peak.

ranges, from 600 to 1100 °C [55], depending on the preparation conditions.

The crystalline sizes and composition phases of the TiO_2 nanoparticles assessed from XRD data are listed in Tables 3 and 4. The percentage of anatase and rutile in the TiO_2 samples studied was determined by using the relative intensity of the maximum intensity peaks for anatase and rutile in the XRD patterns.

These tables show that with the increase in calcination temperature, there is an increase in the anatase crystalline size. The slow growth of anatase crystalline size at 600 °C in TiO_2-AA-600 is attributed to the mixed phase, since this TiO_2 sample calcined at 600 °C is composed of 75% anatase and 25% rutile. With further increasing the calcination temperature, the pattern corresponds to a complete TiO_2 rutile structure, indicating complete phase transformation from anatase to rutile at 800 °C.

As expected, an increase in the calcination temperature results in an increase in the crystallinity. The mean anatase crystalline sizes calculated from the XRD patterns were found to increase from 7 to 32 nm, when the calcination temperature increases up to 600 °C in samples prepared with acetic acid. When isopropanol is used, anatase crystalline sizes range from 6 to 26 nm, for calcination temperatures up to 500 °C.

The effect of calcination temperatures on the composition of anatase and rutile in the nanoparticles of TiO_2-AA and TiO_2-IP is shown in Tables 3 and 4. From them, it can clearly be seen that nucleation and growth of rutile phase initiates at a temperature below 600 °C in TiO_2-AA and a little lower, below 500 °C, in the TiO_2-IP sample. Additionally, the anatase phase is maintained until 700 °C in the sample TiO_2-AA (Table 3), whereas it becomes 100% rutile from 600 °C in TiO_2-IP samples (Table 4). Therefore, the hydrolysis agent influences the crystalline structure and the temperatures at which phase changes occur.

Furthermore, the rutile crystalline size in TiO_2-AA is 35 nm at 600 °C, while it slightly increases to 43 nm when the temperature goes to 800 °C. At this temperature, anatase phase has been totally eliminated and there are only large rutile crystals in the sample.

The choice of catalysts is important to stabilize the anatase phase or to obtain rutile at lower temperatures. Indeed, without changing other preparation parameters, the pure rutile phase is obtained at high temperature (~800 °C) when using acetic acid.

It is difficult to establish the reasons for the differences in anatase–rutile crystallite phase transformation in the treated samples TiO_2-AA and TiO_2-IP. One possible explanation for the higher anatase–rutile transition temperatures when using acetic acid, related with results previously published in the literature by other research teams, would be based on pH differences and on the ability of some of the acetic acid molecules to coordinate to the titania network to produce defects or impurities with different ionic mobility [56]. Acetic acid coordination depends on the degree of cross-linking of the gel structure (that also depends on pH, since it determines the degree of hydrolysis attainable before polymerization, determining the degree of cross-linking of the network) and all this affects the formation of the rutile phase [56].

4.3. Transmission electron microscopy characterization

The morphology of the untreated TiO_2 nanoparticles synthesized by the sol–gel method with different hydrolysis agents is shown in Fig. 1. As shown in the TEM images, the samples consist of the aggregation of nanoparticles. Their mean crystalline sizes are small; around 7 nm for TiO_2-AA (Fig. 1a) and 6 nm for TiO_2-IP (Fig. 1b).

Comparison between Fig. 1a and b show that TiO_2-AA-WT nanoparticles are more crystalline than TiO_2-IP-WT nanoparticles, according to what was also observed from the XRD patterns.

Fig. 2 shows TEM images of TiO_2 nanoparticles treated at different calcination temperatures. It can be seen that the increase in calcination temperatures leads to an increase in the crystalline size of nanoparticles, together with their agglomeration, especially above 500 °C, in agreement with what it was concluded from previous studies [57]. This agglomeration is particularly drastic for temperatures above 500 °C.

4.4. FTIR

Fig. 3a and b show the Fourier transformed infrared (FTIR) spectra of TiO_2 after calcination at different temperatures and Fig. 3c, for comparison purposes, presents the FTIR spectra of untreated TiO_2-AA, TiO_2-IP and Degussa P25.

The broadband peak around 3350–3450 cm^{-1} is attributed to the O—H stretching of physisorbed water on the TiO_2 surfaces [58]. The two strong bands near 2300 cm^{-1}, appearing in the TiO_2-AA samples calcined from 400 to 800 °C, are derived from bidentate carbonate and bicarbonate species [59]. The relatively sharp band

Table 4
Crystalline size and phase composition of TiO_2-IP samples.

Sample	Phase composition	Anatase by XRD (%)	Rutile by XRD (%)	Crystalline size of anatase (nm)[a]	Crystalline size of rutile (nm)[a]
TiO_2-IP-WT	A	100	–	6	–
TiO_2-IP-300	A	100	–	8	–
TiO_2-IP-400	A	100	–	11	–
TiO_2-IP-500	A-R	71	29	26	40
TiO_2-IP-600	R	–	100	–	43
TiO_2-IP-700	R	–	100	–	45
TiO_2-IP-800	R	–	100	–	47

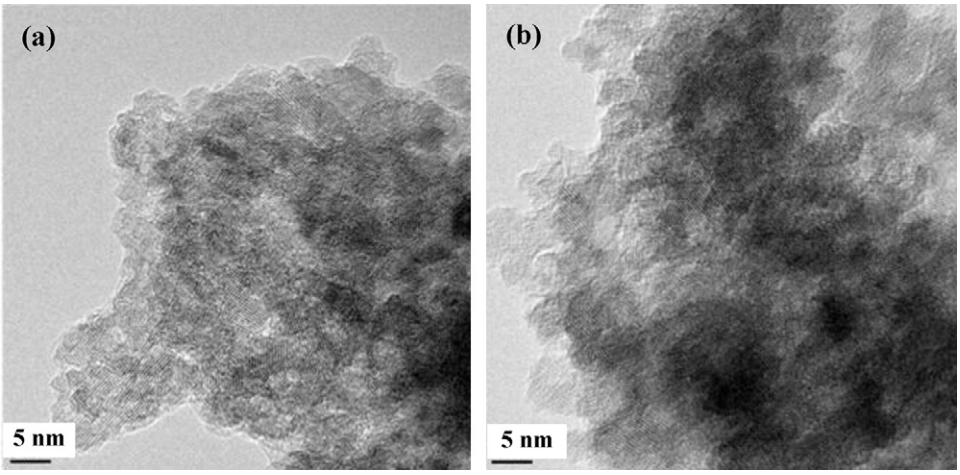

Fig. 1. TEM images of untreated TiO_2 nanoparticles: (a) TiO_2-AA-WT, (b) TiO_2-IP-WT.

at 1637 cm^{-1} corresponds to the O—H bending modes of water molecules [58]. It can be observed (Fig. 3a and b) that there is a significant reduction in the absorbance intensity of these superficial hydroxyl groups with the increase in the calcination temperature, especially above 500–600 °C. At a first glance such loss of surface hydroxyl groups with the temperature treatment could be negative from a photocatalytic point of view [60]. Two weak bands at 1530 cm^{-1} and 1420 cm^{-1}, appearing in the untreated TiO_2 and the treated samples from 400 to 600 °C, are derived from bidentate (chelating or bridging) acetate ligands [59]. The absorption at 1384 cm^{-1} can be assigned to the stretching vibration of —CH_3 groups [58] and the strong absorption observed below 850 cm^{-1} is attributed to lattice vibrations of TiO_2 [58].

The above FTIR spectra clearly show the presence of hydroxyl groups, especially for the untreated samples (TiO_2-AA-WT and TiO_2-IP-WT) and their comparison with the reference material (TiO_2-P25) shows that TiO_2-AA-WT contains the largest amount of hydroxyl groups, what makes it a potential interesting photocatalyst.

5. Photocatalytic activity of TiO_2 nanoparticles

The present section focuses on the results of ambient temperature gas phase propene oxidation with air at low concentration (100 ppmv) in presence of all the different TiO_2 nanoparticles prepared in this work. Additionally, TiO_2-P25 has been used as reference material. Two UV-light sources with maxima wavelengths at 257.7 and 365 nm are analyzed. The 365 nm source was selected to analyze the possibility of using solar light for the photocatalytic oxidation.

5.1. Propene oxidation using a UV-lamp of 257.7 nm

The experiments consisted on first passing the propene stream through the photocatalyst bed until propene concentration in the outlet stream equaled the inlet concentration. Once this occurred, the UV-light was switched on and the decrease in propene concentration in the outlet stream was followed with time, performing at least 3 h tests once the UV-light was switched on. From this type of curves, propene conversion was determined.

Fig. 4 plots the conversion of propene for all the samples prepared using different calcination temperatures obtained with the 257.7 nm UV-lamp at two flow rates (30 and 60 ml/min). It must be remarked that these conversions keep constant for at least 3 h, the holding times used in each catalytic test.

From Fig. 4a and b it can be seen that the calcination temperatures have a significant influence on the photocatalytic activity of the TiO_2-AA and TiO_2-IP nanoparticles for propene oxidation. Thus, in general it can be observed that with the increase in the calcination temperature the activity of TiO_2 nanoparticles decreases significantly.

Focusing on Fig. 4a it can be stated that sample TiO_2-AA-WT is the most active amongst the different samples prepared using AA as hydrolyzing agent. This result can be understood considering the high surface area of this sample, 271 m^2/g, its small primary crystal size, 7.0 nm, and its surface oxygen chemistry. Samples consisting mostly of anatase and treated at temperatures above 300 °C (with lower surface areas and larger crystalline sizes) present a decrease in their photocatalytic activity, according to results previously published [61]. TiO_2-AA-600, which is a mixture of both phases, shows lower photocatalytic activity than TiO_2-AA-WT. This is an important result considering that some previous studies have reported the highest activities for photocatalysts based on the mixture anatase–rutile [62,63]. The fact that TiO_2-AA-600 presents lower photoactivity than, for example, TiO_2-AA-WT can be explained considering that the final activity of the catalysts can be considered as the result of two contributions with opposite effects: on one way the activity itself and, on the other hand, the electron–holes recombination, which is undesirable from a photocatalytic point of view. Thus, although the presence of a mixed phase anatase–rutile leads to a decrease in the electron–holes recombination rate [63], to achieve anatase–rutile mixed-phase material a heat-treatment is required. However, the heat treatment increases the crystalline size and reduces the surface area and the surface oxygen groups' content, and hence produces a decrease in the activity of the materials [64]. In relation to the surface oxygen groups' content, it can be remarked that Fig. 3a has shown a drastic decrease in the —OH groups band for temperatures above 400 °C, which is negative for the activity of these materials.

Thus, in general, the photocatalytic activity of synthesized titania samples decrease with increasing calcination temperatures from 300 to 800 °C, especially when acetic acid is the hydrolyzing agent. It must be recalled that not only the decrease in surface area, pore volume and surface hydroxyl groups and the increase in crystalline size must be considered to understand the decrease in activity. Also, the crystalline phase transformation must be emphasized [65]. The conversions of anatase to rutile, together with the crystalline size enlargement, are negative factors from a photocatalytic point of view [65]. It must be remembered that rutile shows poorer photocatalytic activity than anatase in previously published studies [29–31,65].

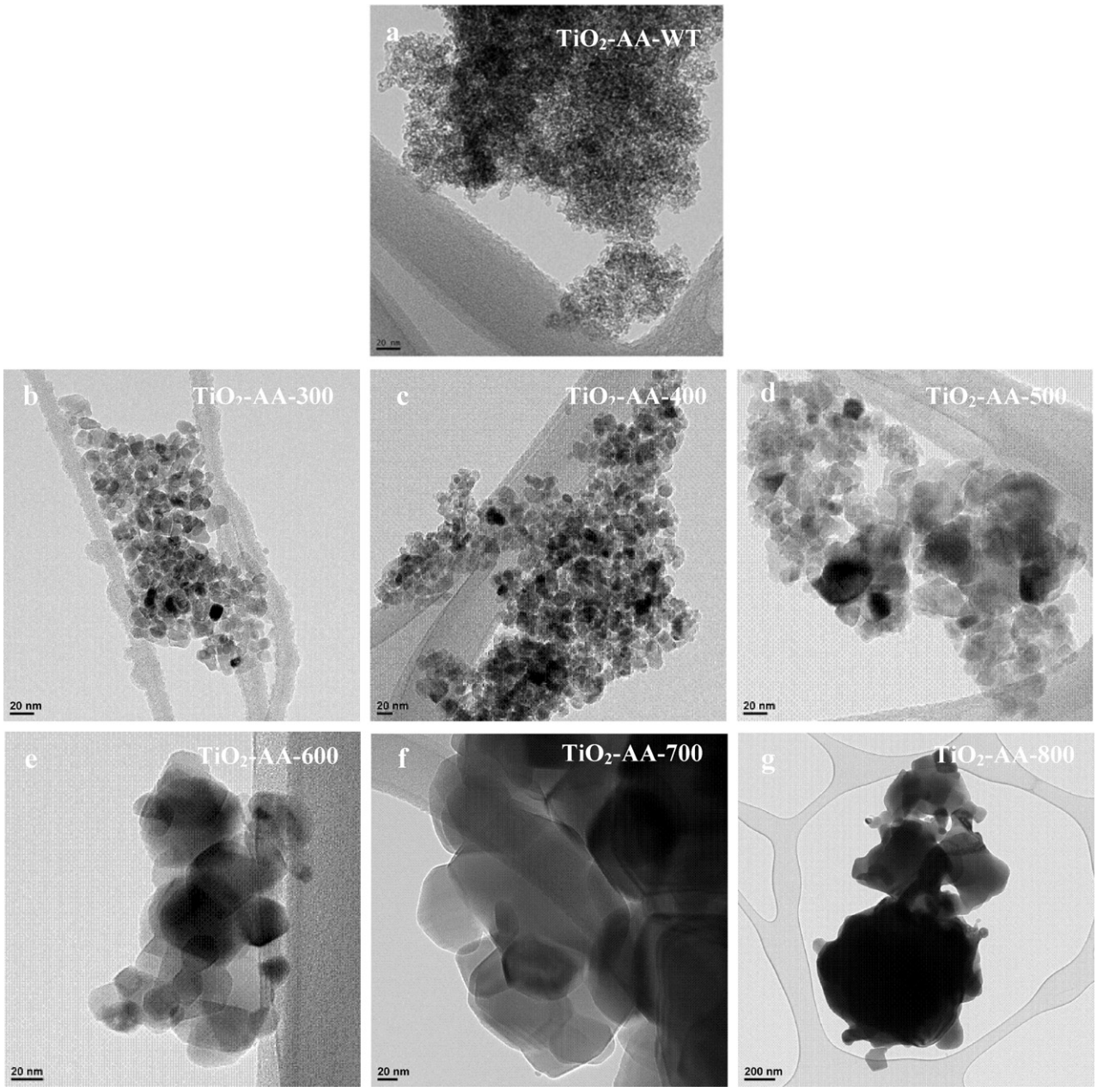

Fig. 2. TEM images of calcined TiO_2-AA nanoparticles at different temperatures: (a) 100 °C; (b) 300 °C; (c) 400 °C; (d) 500 °C; (e) 600 °C; (f) 700 °C and (g) 800 °C.

Focusing on the samples prepared with IP as hydrolyzing agents, Fig. 4b shows that the activities for TiO_2-IP-300 and TiO_2-IP-400 are larger than for TiO_2-IP-WT. These results can be understood considering that isopropanol induces a poor crystallinity in the as-prepared sample TiO_2-IP-WT, as it has been confirmed by XRD in a previous section. It is well-known that crystallinity is another important factor affecting the photocatalytic activity, since the amorphous solids present negligible activity in comparison to crystalline ones [64,66]. Samples prepared with IP at temperature above 300 °C show a small decrease in surface area and a somewhat small increase in their anatase crystalline size which, in principle, would be negative for their activity. However, the thermal treatment leads to an increase in the crystallinity of these samples, responsible for the fact that treated samples TiO_2-IP-300, TiO_2-IP-400 and even TiO_2-IP-500 show larger activities than TiO_2-IP-WT.

In the case of the IP series, as it occurred with AA, the presence of mixed phases anatase–rutile in the photocatalysts is not an advantage in comparison with 100% anatase from a photocatalytic point of view. This is a remarkable result, in agreement with what was concluded when using AA as hydrolyzing agent, and emphasizes the need of large surface area photocatalysts with small anatase crystalline sizes, and also large surface oxygen groups' contents.

Comparison between the photocatalytic activities of the samples prepared with both hydrolyzing agents shows that the samples prepared with AA present, in general, larger activities than those prepared with IP. These large differences between both hydrolyzing agents cannot be explained neither considering porosities of both series of samples (see Tables 1 and 2) nor crystalline sizes and phase compositions (see Tables 3 and 4). Their main differences between these two sets of samples can be attributed to their chemical composition, especially in their surface oxygen chemistry

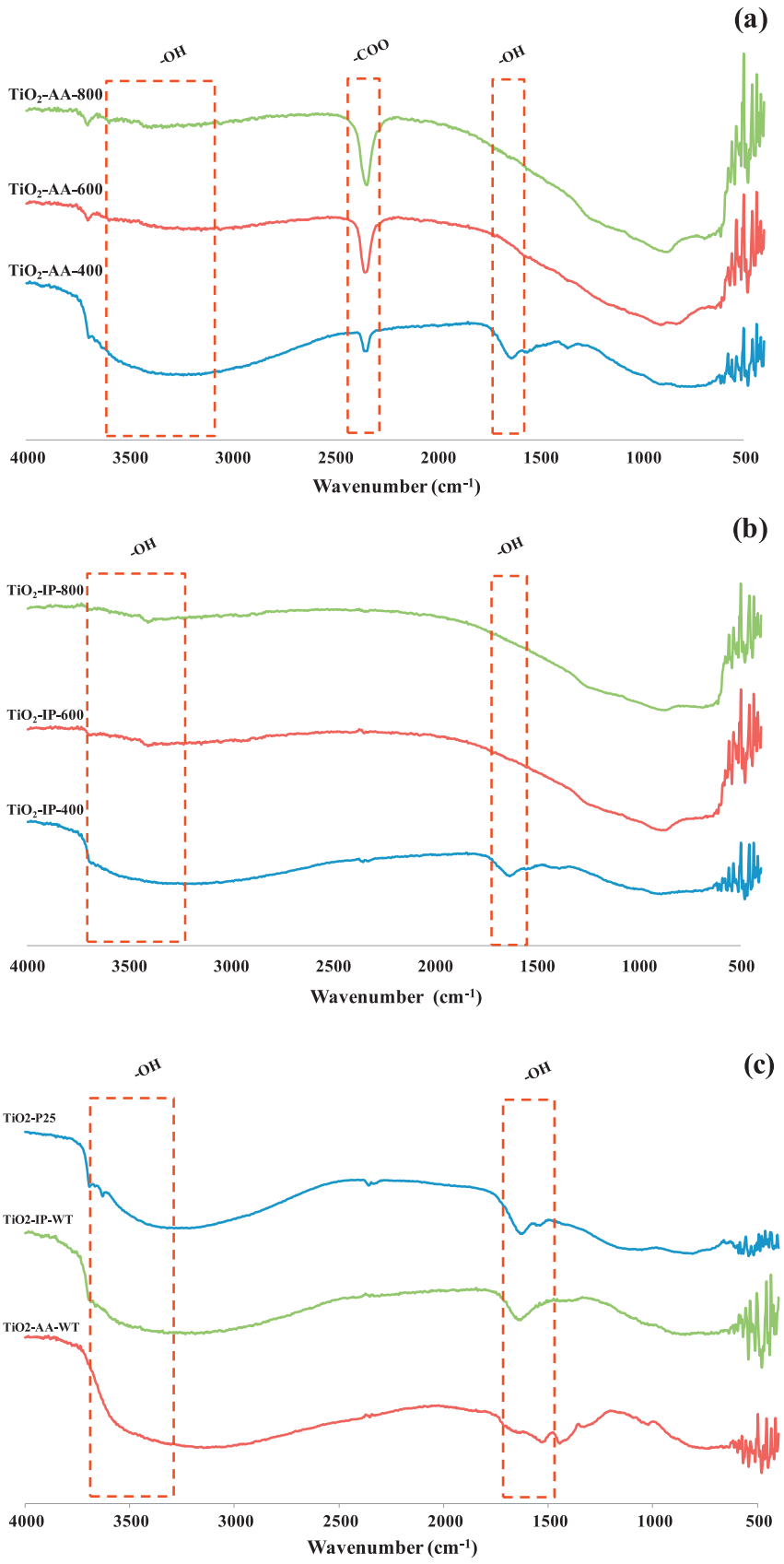

Fig. 3. FTIR spectra of (a) calcined TiO_2-AA nanoparticles; (b) calcined TiO_2-IP nanoparticles and (c) TiO_2 nanoparticles without thermal treatment and Degussa P25.

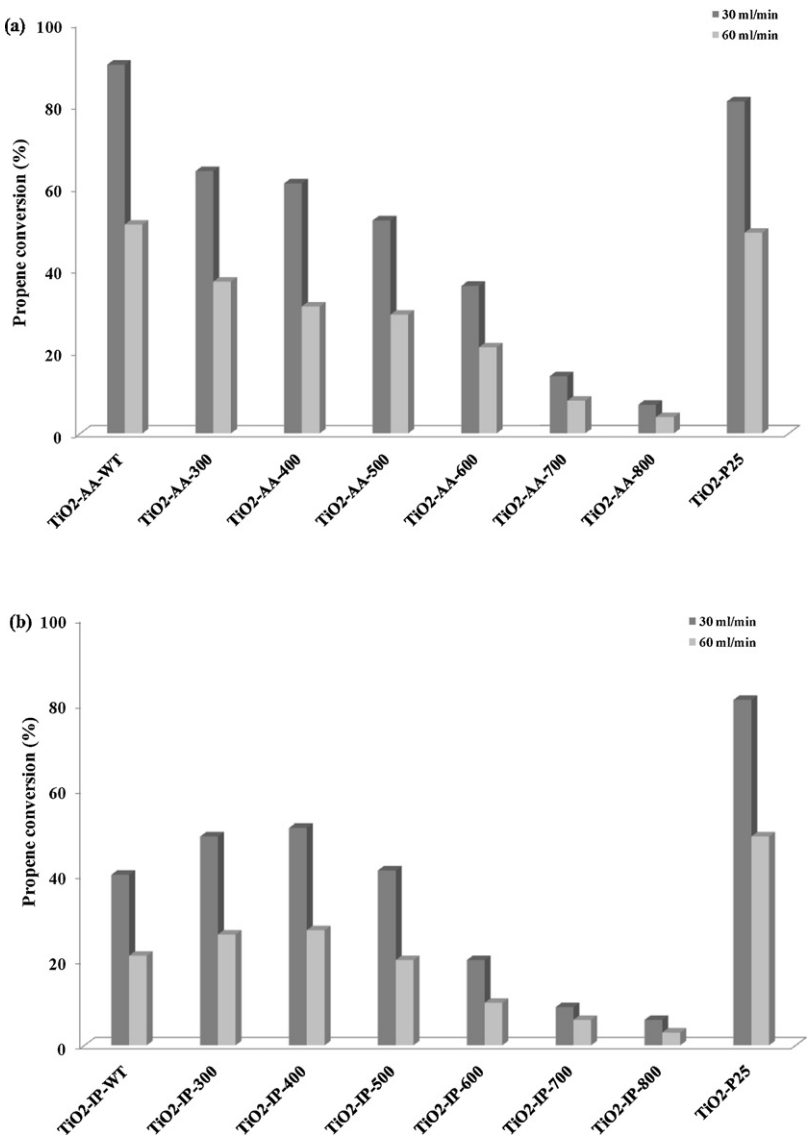

Fig. 4. Propene conversion (at 30 and 60 ml/min) using (a) TiO_2-AA and (b) TiO_2-IP-nanoparticles with the 257.7 nm UV-lamp.

(see Fig. 3a and b), aspect that many papers have claimed to be important [67,68], but whose effect has not been totally clarified yet.

Activity of reference material Degussa TiO_2-P25 was also measured and compared with the different TiO_2 nanoparticles synthesized by the sol–gel method. As it can be seen, the photocatalytic activity of TiO_2-P25 is slightly higher than any of the calcined TiO_2-IP and TiO_2-AA samples, despite the fact that many of the calcined samples present larger surface areas and lower crystalline sizes than P25. Interestingly, the activity of TiO_2-AA-WT under this UV light radiation (UV-C ~ 257.7 nm) is larger than that of P25, which can be attributed to several factors: higher specific surface area, pure and good anatase phase, higher pore volume and larger surface oxygen groups' content. Considering the fact that many of the prepared materials present larger surface area and smaller anatase size than P25, but show lower activity than P25, and the differences between FTIR spectra of TiO_2-AA-WT and Degussa TiO_2-P25 (see Fig. 3c) make us consider that surface oxygen chemistry of TiO_2-AA-WT is responsible of its large activity, which confirms that the surface chemistry of the TiO_2-based photocatalysts plays a very important role. The reason might be that the surface adsorbed water and hydroxyl groups will react with photoexcited holes on the catalyst surface and produce hydroxyl radicals, which are powerful oxidants in the degradation of organic compounds [68].

The results presented let us conclude that the use of acetic acid as hydrolyzing agents is very interesting from the point of view of the final catalytic activity of the prepared nanoparticles since it leads to a highly crystalline material without the need of a calcination treatments, that shows very good catalytic activity. Additionally, it appears that those photocatalysts consisting on anatase phase are more photoactive than those with TiO_2 predominantly on anatase phase but with a small fraction of rutile (<30%).

In these experiments, CO_2 quantification data have shown that at the two different propene flow rates total mineralization of the oxidized propene takes place, according to the following reaction:

$$2C_3H_6 + 9O_2 \rightarrow 6CO_2 + 6H_2O \quad (5)$$

5.2. Propene oxidation using a UV-lamp of 365 nm

As stated before, the use of wavelengths in the range of the solar radiation is of great interest in photocatalysis since it would permit to avoid the use of artificial light for the oxidation of pollutants. In this sense, the present section analyses the use of UV with

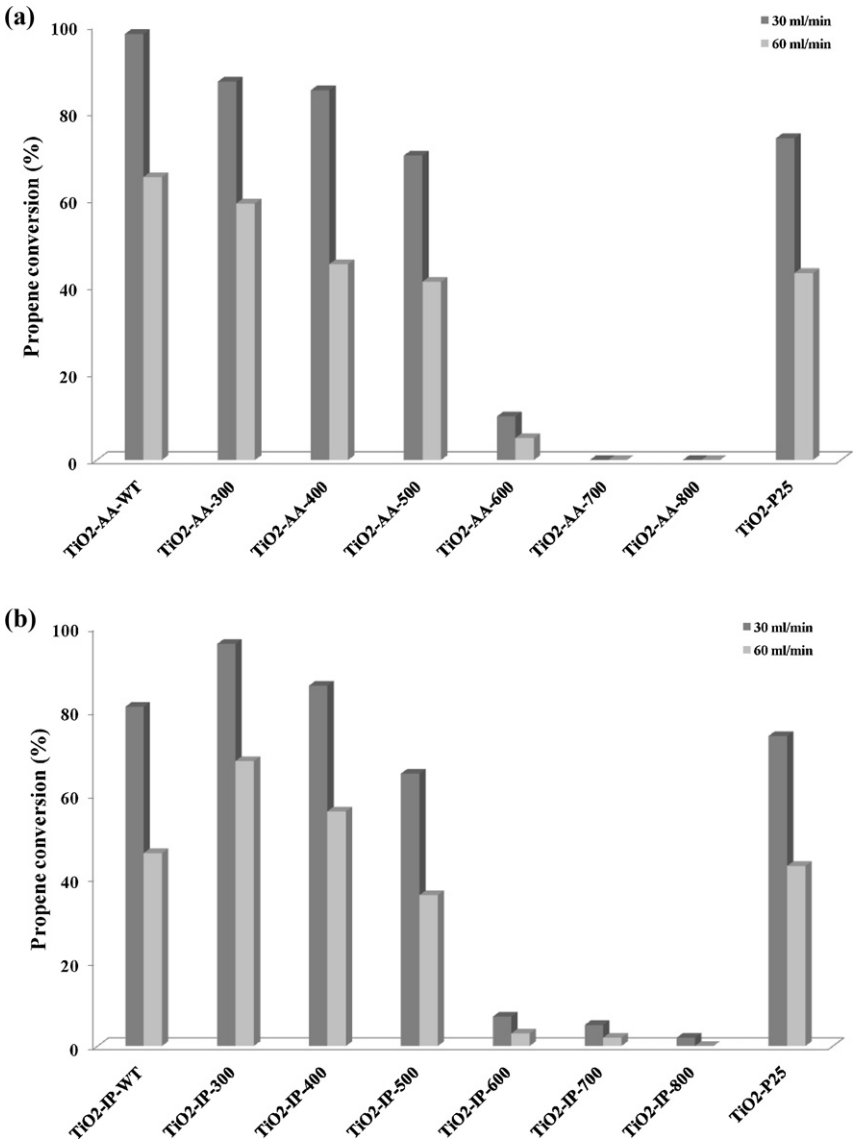

Fig. 5. Propene conversion (at 30 and 60 ml/min) using TiO_2-AA and TiO_2-IP nanoparticles and the 365 nm UV-lamp.

maximum radiation peak at 365 nm and compares these results with those previously reported for UV-light with a maximum peak at 257.7 nm.

Fig. 5 summarizes propene conversions for the 365 nm peak UV-lamp. Let us remember that these conversions keep constant for at least 3 h, which are the holding times used in each catalytic test.

These results show that, as it occurred before, a wide variety of results are shown depending on the selected photocatalyst, and several conclusions can be obtained from these figures and from their comparison with the results in Fig. 4.

Curiously and interestingly, the first and most important conclusion is that a higher oxidation activity for propene is observed when replacing the 257.7 nm by the 365 nm lamp for all TiO_2 nanoparticles prepared, independently of the hydrolyzing agent used. Thus, as an example, an increase in propene oxidation at 60 ml/min flow rate from 64% to 87% is observed in TiO_2-AA-300 and from 49% to 96% is observed in TiO_2-IP-300. This seems to indicate that the use of solar light for low concentration propene oxidation would be more efficient for all the samples studied.

Another important conclusion is that some samples prepared with AA as hydrolyzing agent show again larger activities than those prepared with IP (i.e. compare TiO_2-AA-WT and TiO_2-IP-WT). The differences between these two samples can be explained taking into account the surface chemistry of these samples, shown in the FTIR spectra. However, for other conditions, IP leads to more active materials than AA (i.e. compare TiO_2-AA-300 and TiO_2-IP-300).

In these experimental conditions it can also be observed that the TiO_2-IP sample calcined at 300 °C is more active than TiO_2-IP-WT, due to the increase in crystallinity after the thermal treatment, in agreement with what was observed when using the 257.7 nm source.

CO_2 quantification data have also shown that with this UV light and at the two different propene flow rates, total mineralization of the oxidized propene takes place, according to reaction (5).

In general, with this type of UV source many materials, such as TiO_2-AA-WT, TiO_2-AA-300, TiO_2-IP-300 and TiO_2-IP-400, show very good propene conversions, what highlights the suitability of the preparation method used and the conditions selected for this application.

Also it appears that the photocatalysts consisting on anatase phase are more photoactive than those with TiO_2 predominantly on anatase phase having a small fraction of rutile (<30%). It is observed

again a strong decrease in photocatalytic activity in the samples consisting of rutile, in agreement with previously published results [69].

In the present study, a UVC lamp and UVA lamp were used to compare the effect of two different light sources. The maximum wavelength of the UVC lamp appears at 257.7 nm (emission power 2.1 W), and that of the UVA lamp appears at 365 nm (emission power 1 W). In the case of the reference material TiO_2-P25, a larger activity can be seen with the 257.7 nm lamp, in comparison with the 365 nm one (see Figs. 4 and 5). Similar results have been observed in previous studies. As an example, Kočí et al. studied the photocatalytic reduction of CO_2 by water in the presence of Ag/TiO_2 catalyst under illumination by lamps with different wavelengths (254, 365 and 400 nm) [70]. The yields of the main products were higher with the 254 nm lamp than with the 365 nm lamp, while no products were observed with the 400 nm lamp [70]. This was because the electron–hole generation rate increased with increasing energy of irradiation of the light (decreasing wavelength) and there were higher densities of electron states at higher energies in TiO_2 [70]. The energy of the electrons excited by visible light (400 nm) was too low for CO_2 photocatalytic reduction [70].

Hofstadler et al. also showed that shorter wavelengths resulted in higher photocatalytic degradation process rates of 4-chlorophenol, with small amounts of intermediates being formed [71]. This was attributed to the fact that shorter wavelength is associated with greater photon energy [71]. A last example is that included in the study of Pengyi et al., who studied the effect of ultraviolet light wavelength on the decomposition of toluene by O_3/UV, TiO_2/UV and O_3/TiO_2/UV processes [72]. It was found that in all these three processes the conversion irradiated with 254 nm UV lamps was much higher than that with 365 nm [72]. In the O_3/TiO_2/UV process, 92.5% of toluene was decomposed when irradiated with 254 nm UV lamps, while only 63.5% was decomposed when irradiated with 365 nm UV lamps [72]. The significant differences resulted from 254 and 365 nm UV lamps are mainly due to the fact that the 254 nm lamp irradiated stronger UV intensity (58 W/m^2) than the 365 nm one (30 W/m^2) [72]. Thus, much more photons with higher energy were irradiated by the 254 nm UV lamp, which can basically explain why the TiO_2/UV was much more efficient with 254 nm UV lamp than with 365 nm lamp [72].

However, on the contrary, in most prepared samples, especially in those without thermal treatment or treated at low temperatures, the UV-A lamp (365 nm) showed higher photocatalytic degradation than the UV-C lamp (compare Figs. 4 and 5). This implies that there is not an optimum radiation for the all the materials, but it depends on the photocatalyst, being P25 more effective with the UV-C lamp and most of the prepared materials more effective with the UV-A one.

This is, in principle, difficult to understand since each photon with enough energy can produce only one electron–hole couple. However, it could be interpreted considering the different particle sizes or different aggregates sizes and their corresponding different scattering effect.

Additionally, it has been observed that for samples prepared without thermal treatment or at low temperature ones, in case of UV-C the conversion is doubled when flow is divided by two, whereas in case of UV-A it is not doubled, which implies differences in the reaction order when using the different wavelengths. These are all very interesting points which will be further investigated in following studies.

6. Conclusions

In this study, crystalline titanium dioxide nanoparticles were directly synthesized by sol–gel method at low temperature using two hydrolyzing agents, acetic acid or isopropanol. By calcination of the as-prepared TiO_2 at different temperatures anatase, mixed phase (anatase and rutile), and rutile TiO_2 samples were prepared. With increasing the calcination temperature, the specific surface areas of the as-prepared TiO_2 samples decrease, and TiO_2 precursor undergoes the phase transformation of $A \rightarrow A + R \rightarrow R$.

From our results, it is shown that those photocatalysts, consisting predominantly on anatase phase, are more photoactive than those with a small fraction of rutile (<30%) or only rutile, for both hydrolyzing agents.

The maximum photocatalytic oxidation activity has been achieved with the sample prepared with acetic acid without additional heat-treatments (TiO_2-AA-WT). The interesting activity of this sample can be attributed to several factors: high specific surface area, highly crystalline anatase phase, high pore volume and large surface oxygen groups' content.

For samples prepared with acetic acid, the activity falls down when increasing heat treatment temperatures, due to crystal size increases, surface area decreases and surface oxygen groups' content decreases as well. As an example, sample TiO_2-AA-800, with 100% rutile phase, does not show photoactivity.

The sample prepared with isopropanol without additional heat-treatments (TiO_2-IP-WT) shows lower crystallinity and lower oxygen surface groups' content than TiO_2-AA-WT, and hence, worse photocatalytic performance. Some samples prepared from IP by heat treatment (samples TiO_2-IP-300 and TiO_2-IP-400) present larger activity than TiO_2-IP-WT, possibly due to an increase in crystallinity, although higher temperature than 400 °C decreases the activity, as in the case of acetic acid.

The use of different UV lights presents a marked impact on the photocatalytic activity of propene at low concentration (100 ppmv). Most of the samples have suitable photoactivities, many of them higher than TiO_2-P25. Surprisingly, and interestingly, their photoactivities are better with 365 nm radiation than with 257.7 nm, in contrast to what happens with Degussa and with most results from the literature. Especially remarkable is the TiO_2 prepared with acetic acid, which possesses very high activity for the photocatalytic oxidation of propene at low concentration (100 ppmv), particularly better with the 365 nm radiation.

Acknowledgments

M. Ouzzine thanks MAEC-AECID for a predoctoral fellowship. The authors thank Generalitat Valenciana (Prometeo/2009/047 and FEDER), and Office for Research, Development and Innovation of University of Alicante (UAUSTI10-08) for financial support.

References

[1] O. Kleinschmidt, D. Hesse, Canadian Journal of Chemical Engineering 80 (2002) 71–78.
[2] W. Wang, L.W. Chaing, Y. Ku, Journal of Hazardous Materials B 101 (2003) 133–146.
[3] H. Chen, S.W. Lee, T.H. Kim, B.Y. Hur, Journal of the European Ceramic Society 26 (2006) 2231–2239.
[4] N. Djeghri, S.J. Teichner, Journal of Catalysis 62 (1980) 99–106.
[5] J.M. Herrmann, W. Mu, P. Pichat, Heterogeneous Catalysis and Fine Chemicals 2 (1991) 405–412.
[6] D.S. Muggli, L. Ding, Applied Catalysis B: Environmental 32 (2001) 181–194.
[7] M. Anpo, K. Chiba, M. Tomonari, S. Coluccia, M. Che, M.A. Fox, Bulletin of the Chemical Society of Japan 64 (1991) 543–551.
[8] M. Fujihira, Y. Satoh, T. Osa, Nature 293 (1981) 206–208.
[9] J. Peral, D.F. Ollis, Journal of Catalysis 136 (1992) 554–565.
[10] A.J. Maira, K.L. Yeung, C.Y. Lee, P.L. Yue, C.K. Chan, Journal of Catalysis 192 (2000) 185–196.
[11] H. Fontane, M. Veillerot, J.C. Gallo, R. Guillermo, Proceedings of the 8th International Symposium on Transport and Air Pollution, Graz, 1999.
[12] E. Rivière, CITEPA Report, Paris, 1998.
[13] F. Mühlberger, T. Streibel, J. Wieser, A. Ulrich, R. Zimmermann, Analytical Chemistry 77 (2005) 7408–7414.

[14] C.T. Brigden, S. Poulston, M.V. Twigg, A.P. Walker, A.J.J. Wilkins, Applied Catalysis B: Environmental 32 (2001) 63–71.
[15] M.A. Lillo-Ródenas, N. Bouazza, A. Berenguer-Murcia, J.J. Linares-Salinas, P. Soto, A. Linares-Solano, Applied Catalysis B: Environmental 71 (2007) 298–309.
[16] N. Bouazza, M.A. Lillo-Ródenas, A. Linares-Solano, Applied Catalysis B: Environmental 77 (2008) 284–293.
[17] N. Bouazza, M.A. Lillo-Ródenas, A. Linares-Solano, Applied Catalysis B: Environmental 84 (2008) 691–698.
[18] N. Bouazza, M. Ouzzine, M.A. Lillo-Ródenas, A. Linares-Solano, Applied Catalysis B: Environmental 92 (2009) 377–383.
[19] M. Ouzzine, M.A. Lillo-Ródenas, A. Linares-Solano, Applied Catalysis B: Environmental 127 (2012) 291–299.
[20] A. Fujishima, T.N. Rao, D.A. Tryk, Journal of Photochemistry and Photobiology C: Photochemistry Review 1 (2000) 1–21.
[21] A. Fujishima, X. Zhang, Comptes Rendus Chimie 9 (2006) 750–760.
[22] Y.F. Chen, C.Y. Lee, M.Y. Yeng, H.T. Chiu, Materials Chemistry and Physics 81 (2003) 39–44.
[23] D. Chatterjee, A. Mahata, Applied Catalysis B: Environmental 33 (2001) 119–125.
[24] N. Serpone, P. Maruthamuthu, P. Pichat, E. Pelizzetti, H. Hidaka, Journal of Photochemistry and Photobiology Chemistry 85 (1995) 247–255.
[25] A.V. Pérez, J. Ma, A. Girón, Radiación Infrarroja y Ultravioleta, in: Serie Electrotecnologías, Mc GrawHill/Interamericana de España, S.A.U., 1998, pp. 240.
[26] J.A. Cortés, M.T. Alarcón-Herrera, M. Villicaña-Méndez, J. González- Hernández, J.F. Pérez-Robles, Environmental Progress & Sustainable Energy 30 (2011) 318–325.
[27] R.I. Bickley, J.S. Lees, L. Palmisano, Journal of Solid State Chemistry 92 (1991) 178–190.
[28] Q. Zhang, L. Gao, J. Guo, Applied Catalysis B: Environmental 26 (2000) 207–215.
[29] A.L. Linsebigler, G.Q. Lu, J.T. Yates, Chemical Reviews 95 (1995) 735–758.
[30] G.M. Zuo, Z.X. Cheng, H. Chen, G.W. Li, T. Miao, Journal of Hazardous Materials 128 (2006) 158–163.
[31] C. Hägglund, B. Kasemo, L. Österlund, Journal of Physical Chemistry B 109 (2005) 10886–10895.
[32] S.S. Watson, D. Beydoun, J.A. Scott, R. Amal, Chemical Engineering Journal 95 (2003) 213–220.
[33] A. Mills, N. Elliott, G. Hill, D. Fallis, J.R. Durrant, R.L. Willis, Photochemical and Photobiological Sciences 2 (2003) 591–596.
[34] R.R. Bacsa, J. Kiwi, Applied Catalysis B: Environmental 16 (1998) 19–29.
[35] J.M. Warson, A.T. Cooper, J.R.V. Flora, Environmental Engineering Science 22 (2005) 666–675.
[36] A. Sclafani, L. Palmisano, M. Schiavello, Journal of Physical Chemistry 94 (1990) 829–832.
[37] K. Tanaka, M.F.V. Capule, T. Hisanaga, Chemical Physics Letters 187 (1991) 73–76.
[38] J. Jiang, D.R. Chen, P. Biswas, Nanotechnology 18 (2007) 285603–285611.
[39] P. Worathanakul, J.K. Jiang, P. Biswas, P. Kongkachuichay, Journal of Nanoscience and Nanotechnology 8 (2008) 6253–6259.
[40] K.K. Latt, T. Kobayashi, Ultrasonics Sonochemistry 15 (2008) 484–491.
[41] Y.V. Kolenko, V.D. Maximov, A.A. Burukhin, V.A. Muhanov, B.R. Churagulov, Materials Science and Engineering C 23 (2003) 1033–1038.
[42] C.S. Kim, B.K. Moon, J.H. Park, S.T. Chung, S.M. Son, Journal of Crystal Growth 254 (2003) 405–410.
[43] H.D. Nam, B.H. Lee, S.J. Kim, C.H. Jung, J.H. Lee, S. Park, Japanese Journal of Applied Physics 37 (1998) 4603–4608.
[44] H. Kominami, J.-I. Kalo, Y. Takada, Y. Doushi, B. Ohtani, S.-I. Nishimoto, M. Inoue, Y. Kera, Catalysis Letters 46 (1997) 235–240.
[45] L. Sifang, Y. Guoliang, C. Guoqin, Journal of Physical Chemistry C 113 (2009) 4031–4037.
[46] A.R. Liu, S.M. Wang, Y.R. Zhao, Z. Zheng, Materials Chemistry and Physics 99 (2006) 131–134.
[47] N. Wetchakun, S. Phanichphant, Current Applied Physics 8 (2008) 343–346.
[48] Y.G. Chen, D.D. Dionysiou, Journal of Molecular Catalysis A 244 (2006) 73–82.
[49] N. Venkatachalam, M. Palanichamy, V. Murugesan, Materials Chemistry and Physics 104 (2007) 454–459.
[50] H. Zhang, J.F. Banfield, Journal of Physical Chemistry B 104 (2000) 3481–3487.
[51] R.A. Spurr, H. Myers, Analytical Chemistry 29 (1957) 760–762.
[52] J. Rouquerol, F. Rouquerol, K.S.W. Sing, Adsorption by Powders and Porous Solids: Principles, Methodology and Applications, Academic Press, San Diego, 1999.
[53] A. Linares-Solano, J. Alcañiz-Monje, C. Salinas-Martínez de Lecea, D. Cazorla-Amorós, Transo 185 (1998) 316–325.
[54] S.-J. Kim, S.-D. Park, Y.H. Jeong, S. Park, Journal of the American Ceramic Society 82 (1999) 927–932.
[55] J. Ovenstone, K. Yanagisawa, Chemistry of Materials 11 (1999) 2770–2774.
[56] D. Bersani, R. Capelleti, P.P. Lottici, G. Gnappi, A. Montenero, Materials Science Forum 87 (1997) 239–241.
[57] K. Nagaveni, M.S. Hegde, N. Ravishankar, G.N. Subbanna, G. Madras, Langmuir 20 (2004) 2900–2907.
[58] M. Janus, B. Tryba, E. Kusiak, T. Tsumura, M. Toyoda, M. Inagaki, A.W. Morawski, Catalysis Letters 128 (2009) 36–39.
[59] S. Doeuff, M. Henry, C. Sanchez, J. Livage, Journal of Non-Crystalline Solids 89 (1987) 206–216.
[60] S.H. Szczepankiewicz, A.J. Colussi, M.R. Hoffmann, Journal of Physical Chemistry B 104 (2000) 9842–9850.
[61] K. Lv, Q. Xiang, J. Yu, Applied Catalysis B: Environmental 104 (2011) 275–281.
[62] L. Shi, D. Weng, Journal of Environmental Sciences 20 (2008) 1263–1267.
[63] T. Ohno, K. Sarukawa, K. Tokieda, M. Matsumura, Journal of Catalysis 203 (2001) 82–86.
[64] D.S. Kim, S.-Y. Kwak, Applied Catalysis A: General 323 (2007) 110–118.
[65] K.Y. Jung, S.B. Park, S.-K. Lhm, Applied Catalysis A: General 224 (2002) 229–237.
[66] Z. Qinghong, G. Lian, G. Jingkun, Applied Catalysis B: Environmental 26 (2000) 207–215.
[67] C.S. Turchi, D.F. Ollis, Journal of Catalysis 122 (1990) 178–192.
[68] Z. Ding, G.Q. Lu, P.F. Greenfield, Journal of Physical Chemistry B 104 (2000) 4815–4820.
[69] E. Pulido Melián, O. González Díaz, J.M. Doña Rodríguez, G. Colón, J.A. Navío, J. Pérez Peña, Applied Catalysis A: General 411–412 (2012) 153–159.
[70] K. Kočí, K. Zatloukalová, L. Obalová, S. Krejčiková, Z. Lacný, L. Čapek, A. Hospodková, O. Šolocová, Chinese Journal of Catalysis 32 (2011) 812–815.
[71] K. Hofstadler, R. Bauer, S. Novalic, G. Heisler, Environmental Science and Technology 28 (1994) 670–674.
[72] Z. Pengyi, L. Fuyan, Y. Gang, C. Qing, Z. Wanpeng, Journal of Photochemistry and Photobiology A 156 (2003) 189–194.